Received: 10 August 2022 | Revised: 12 October 2022 | Accepted: 23 November 2022

DOI: 10.1002/jex2.68

SHORT COMMUNICATION

Lipoprotein particles exhibit distinct mechanical properties

Melissa C. Piontek | **Wouter H. Roos**

Moleculaire Biofysica, Zernike Instituut, Rijksuniversiteit Groningen, Groningen, The Netherlands

Correspondence
Wouter H. Roos, Moleculaire Biofysica, Zernike Instituut, Rijksuniversiteit Groningen, 9747 AG Groningen, The Netherlands.
Email: w.h.roos@rug.nl

Funding information
Nederlandse Organisatie voor Wetenschappelijk Onderzoek, Grant/Award Numbers: STW Perspectief Cancer-ID 14192, Vidi grant

Abstract
Lipoproteins (LPs) are micelle-like structures with a similar size to extracellular vesicles (EVs) and are therefore often co-isolated, as intensively discussed within the EV community. LPs from human blood plasma are of particular interest as they are responsible for the deposition of cholesterol ester and other fats in the artery, causing lesions, and eventually atherosclerosis. Plasma lipoproteins can be divided according to their size, density and composition into chylomicrons (CM), very-low-density lipoproteins (VLDL), low-density lipoproteins (LDL) and high-density lipoproteins (HDL). Here, we use atomic force microscopy for mechanical characterization of LPs. We show that the nanoindentation approach used for EV analysis can also be used to characterize LPs, revealing specific differences between some of the particles. Comparing LPs with each other, LDL exhibit a higher bending modulus as compared to CM and VLDL, which is likely related to differences in cholesterol and apolipoproteins. Furthermore, CM typically collapse on the surface after indentation and HDL exhibit a very low height after surface adhesion both being indications for the presence of LPs in an EV sample. Our analysis provides new systematic insights into the mechanical characteristics of LPs.

KEYWORDS
atomic force microscopy (AFM), chylomicrons (CM), high-density lipoproteins (HDL), lipoproteins (LPs), low-density lipoproteins (LDL), mechanical properties, very-low-density lipoproteins (VLDL)

1 | INTRODUCTION

Lipoproteins (LPs) are nano-sized particles synthesized by the liver as well as the intestine. Surrounded by a single layer of phospholipids with outward facing hydrophilic head, cholesterol and apolipoproteins, the hydrophobic core of LPs is filled with triacylglycerides and cholesterol esters. This structure makes LPs ideal candidates for the transport of phospholipids, cholesterol and triacylglycerides within the body. LPs transporting these substances can be extracted from human blood plasma and can be divided into several subclasses: chylomicrons (CM), very-low-density lipoproteins (VLDL), low-density lipoproteins (LDL) and high-density lipoproteins (HDL). Figure 1 shows schematic representations of these particle types alongside some characteristics, for example composition and density. Due to the size and density overlap with extracellular vesicles (EVs) LPs are often co-isolated when working with EVs. Such contaminated samples are being intensively discussed within the EV community (Simonsen, 2017; Sódar et al., 2016; Théry et al., 2018). Isolation, identification and characterization of different subpopulations of particles in plasma, such as tumor-derived EVs, platelet-derived EVs and LPs is challenging. These challenges have various reasons: EVs and LPs are heterogeneous, there is limited knowledge on the chemical composition of EVs, the number of lipoproteins in blood outnumber EVs and isolation methods do not effectively separate EVs from LPs nor are they well-standardized (Coumans et al., 2017; Ramirez et al., 2018; Théry et al., 2018; van der Pol et al., 2014). The isolation protocol used determines the separation quality of EVs and LPs (Busatto et al., 2022). Currently, isolation procedures combining ultracentrifugation and

	CM	VLDL	LDL	HDL
Lipids (hydrophilic head) Apolipoprotein	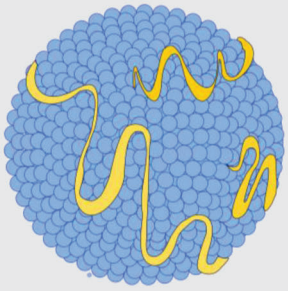			
Triglycerides	90 %	54 %	4 %	1-5 %
Protein	2-3 %	10 %	23 %	35-56 %
Phospholipids	5 %	16 %	21 %	23-35 %
Cholesterol & cholesteryl esters	3 %	20 %	52 %	18-30 %
Major apolipoproteins	Apolipoprotein A, B-48, C, E	Apolipoprotein B-100, C, E	Apolipoprotein B-100	Apolipoprotein A & C
Density (g/ml)	<0.95	0.95-1.006	1.006-1.063	1.063-1.210

FIGURE 1 Schematic representation of different LPs, their major components and the density of the LP classes investigated in this study. Numbers are reproduced from (Kostner & Laggner, 2019). Schematic representations are inspired by (Chiva-Blanch & Badimon, 2019). CM: Chylomicrons; VLDL: very-low density lipoproteins; LDL: low-density lipoproteins; HDL: high-density lipoproteins

size-exclusion chromatography are recommended to obtain the most reliable sample separation (Théry et al., 2018). Additional techniques such as western blot can be used to identify specific LP markers, for example ApoB-100 as LDL marker and ApoA-I as HDL marker to validate/exclude the presence of LPs (Sun et al., 2019). Alongside with EVs, which are composed of a lipid double-layer surrounding their hydrophilic core, LPs are widely studied. Next to studies of the function of LPs, they are studied as markers in therapy, as potential drug delivery vehicles, for example for cancer treatment (Chaudhary et al., 2019), for their role in viral infections, for example SARS-CoV-2 (Kocar et al., 2021), and for their relation to atherosclerotic cardiovascular disease (Pownall et al., 2021). Despite extensive research on the role and metabolism of LPs, the knowledge on mechanical properties of these particles remains limited.

In order to fill this gap and to compare LPs mechanical properties to that of EVs, we apply an atomic force microscopy (AFM) nanoindentation approach (Roos et al., 2010; Vorselen et al., 2017, 2018). Recently, this method was used to describe the mechanical behavior of liposomes (Vorselen et al., 2018), red blood cell EVs in healthy and diseased state (Vorselen et al., 2018), as well as liposomes with membrane-associated proteins (Sorkin et al., 2020), by a Canham-Helfrich theory-based indentation model (Vorselen et al., 2017). Here, we used this approach to systematically investigated the mechanics of CM, VLDL, LDL and HDL from human blood plasma. It allowed for single particle investigation of LPs, providing information about their morphology as well as their stiffness and bending moduli. In addition, the behavior of LPs during indentation was compared to the behavior of previously investigated EVs. We confirm the expected size differences of the various LP samples and reveal a higher bending modulus of LDL compared to VLDL and CM. The small size of HDL excluded the determination of their bending modulus. Comparing these results with previously published data on the size and mechanics of EVs (Sorkin et al., 2018; Vorselen et al., 2018), we observe qualitative and quantitative differences as well as similarities between EVs and LPs.

2 | MATERIALS AND METHODS

Lipoprotein samples. Different types of LPs were purchased as stated below and kindly provided to us by Leon Terstappen and Agustin Enciso-Martínez (Universiteit Twente, The Netherlands). All types of LPs were acquired from human blood plasma. CM were purchased from Sigma-Aldrich Chemie N.V., The Netherlands (SRP6304) with a purity of ≥ 95 % (SDS-PAGE), as specified by the provider. VLDL were purchased from Sigma-Aldrich Chemie N.V., The Netherlands (437,647) with a purity of ≥ 95 % of total LP content by electrophoresis, as specified by the provider. LDL were purchased from Merck KGaA, Darmstadt, Germany (437644) with a purity of ≥ 95 % of total lipoprotein content by electrophoresis, as specified by the provider. HDL sample had a purity of ≥ 95 % (SDS-PAGE), as stated in the manufacturer's specifications, and were purchased from Sigma-Aldrich Chemie N.V., The Netherlands (L8039).

AFM experiments were conducted as previously reported (Vorselen et al., 2017, 2020). In brief: LPs were deposited on poly-L-lysine (PLL) coated glass coverslips. The coverslips were immersed in a 96 % ethanol, 3 % concentrated HCl solution for 10 min in order to clean the coverslip. Hereafter, the coverslips were coated for 1 h in a 0.001 % poly-L-lysine (Sigma) solution. This step was followed by two times rinsing with ultrapure water and final drying at 37°C overnight (at least for 5–6 h). The coated coverslips were stored at 7°C and used within 1 month.

A PLL-coated coverslip was glued to a glass slide using conventional transparent superglue. Next a glass ring was glued on top of the coverslip using JPK bio-compatible glue (Bruker) in order to build a chamber to hold the liquid in place. CM, VLDL and LDL samples were 120x diluted with freshly filtered PBS (0.2 μm polyetersulfone membrane filters from VWR International (catalogue number: 28145–501)). The HDL sample was diluted 240x with freshly filtered PBS. The sample was mixed gently by pipetting. Next 10 μl of sample was added onto the center of the PLL-coated glass coverslip. The chamber was filled with freshly filtered PBS, which serves as imaging buffer. The lipoproteins were imaged in QI™ mode (quantitative imaging mode) on a JPK NanoWizard Ultra Speed setup situated on an inverted microscope (Olympus IX83). The force set point during imaging was typically < 100 pN, pixel time was set to 8.0 ms and z-length was typically set to 40 nm. Imaging was performed at room temperature (~22°C). After imaging a single particle completely, half an image was captured to validate the position of the particle before once indenting its center with a maximum force of 0.4-0.5 nN, and then directly multiple times with higher forces (5-6 nN). The extend speed of the cantilever during indentation was set to 0.3 μm/s throughout all experiments. The sampling rate was set to 1024 Hz and the z-loop was closed. Please note, that during some experiments the 'low force' indentation was not recorded as it was observed that the particles collapse during retraction of the tip. Both before and after indentation of the particle, the tip was checked for contamination (e.g. proteins, lipids) by recording the cantilever response by pushing it on the glass surface until a set force of ~6 nN was reached, while recording a force distance curve. A non-linear response typically indicates contamination on the tip. After indentation, another image was recorded to check for movement or collapse/changes of the particle. Quartz-like cantilevers (qp-BioAC, Nanosensors) with a nominal stiffness of 0.06 N/m and tips with a nominal tip radius < 10 nm were used. Individual cantilevers were calibrated by using thermal tuning.

AFM image analysis was performed as previously reported (Vorselen et al., 2017, 2020). Both images and force curves were processed using JPK Data Processing Software (version 6.1.131). Cross sections were taken for each particle along the fast-scanning axis in order to analyze the shape and the size of the particle. Circular arcs were fit to the data above half of the maximum height to obtain the radius of curvature R_c and the height of the particle. The tip radius was subtracted (10 nm as provided by the manufacturer). Recorded force distance curves were corrected for the offset and subsequently the data was exported and further analyzed in Origin (version 2019). The radius R_0 of the particles in solution was calculated under the assumption of surface area conservation as described previously (Vorselen et al., 2017).

AFM FDC analysis was performed as previously reported (Vorselen et al., 2017, 2020). In brief: The cantilever response was measured on the PLL-coated glass surface and fitted linearly. The resulting fit was subtracted from the measured response when indenting lipoproteins, to obtain force indentation curves (FDCs, see also Vorselen et al., 2020). Due to interference in the baseline of the recorded force distance curves, the contact point was determined manually during offset correction. The height obtained from the arc fit (AFM image) was compared to the height obtained from the force indentation curve to verify indention of the particle's center. The height from the force indentation curve was obtained by determining the distance from contact point, when the tip touches the particle, until pushing on the substrate (see also Vorselen et al., 2020). The stiffness of LPs was found by fitting a straight line in the interval between 0.02 and 0.1 R_c. For finding the tether force two lines with slope 0 were fit to the last detachment of the tether in the retraction curve before reaching the baseline again. The difference of the two intersects was calculated and identified as tether force. Only adhesion events extending beyond the contact point were included. Tethers with forces > 0.25 nN were excluded, since they could correspond to double tethers, as reported previously (Vorselen et al., 2018). For fitting to the theory, described in detail elsewhere (Vorselen et al., 2017), the sum of the squared log Euclidian distance between the theoretical curve and the individual experimental data points was then minimized by adjusting κ as a single fitting parameter. Confidence intervals were estimated using the bias corrected percentile method with 500 bootstrapping repetitions, for which a set of observed value combinations equal in size to the original data set was randomly drawn and fitted.

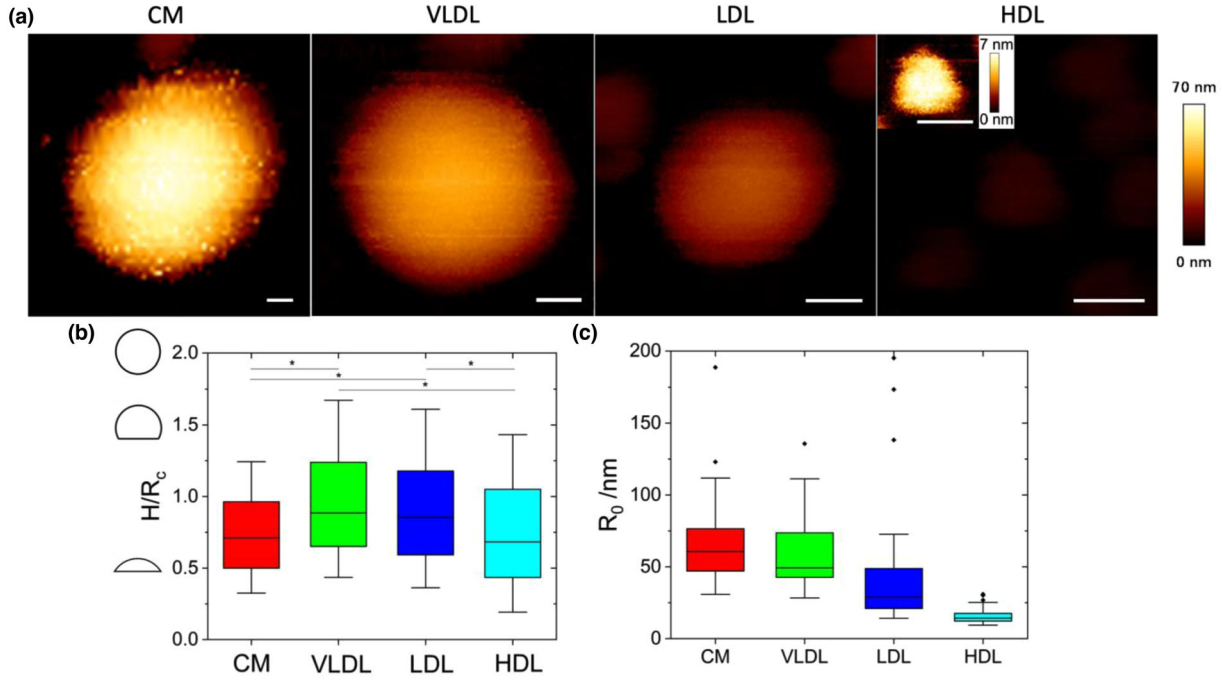

FIGURE 2 Geometry of lipoprotein particles. **(a)** Atomic force microscopy (AFM) topography images of single LPs on glass coverslips coated with poly-L-lysine. Color scale ranges from 0 to 70 nm in all images. Scale bars are 20 nm. Inset in HDL panel shows a zoom in on the particle with a color scale ranging from 0 to 7 nm. **(b)** Average shape of lipoproteins defined by their height (H) over radius of curvature (R_c): 0.73 ± 0.02 (s.e.m., $N = 97$ CM particles), 0.95 ± 0.04 (s.e.m., $N = 56$ VLDL particles), 0.88 ± 0.05 (s.e.m., $N = 40$ LDL particles) and 0.74 ± 0.04 (s.e.m., $N = 75$) for CM, VLDL, LDL and HDL, respectively. Boxplots are shown in which the line within the box indicates median, box limits indicate upper and lower quartiles and whiskers indicate 1.5× interquartile range. Reference shapes are shown in black for H/R_c equals 0.5, 1.5 and 2. * indicates significant differences (two-sided t-test ($p = 0.05$)). **(c)** Calculated radii R_0 of the LPs in solution (before substrate adhesion). CM: Chylomicrons; VLDL: very-low density lipoproteins; LDL: low-density lipoproteins; HDL: high-density lipoproteins

3 | RESULTS

3.1 | AFM imaging of LPs

Atomic force microscopy (AFM) was used to image LPs at high resolution allowing for the determination of the particle geometry and center. Figure 2a shows typical AFM topography images of single LPs (for AFM images of larger scan areas see Supplementary Figure 1), demonstrating that the adhered LPs stay in a shape of a sphere-like cup, as reported previously for EVs and liposomes (Sorkin et al., 2020; Vorselen et al., 2018, 2018). To quantify the shape of LPs, a correction for the tip shape was applied and the ratio of height over radius of curvature was determined yielding an estimation for the particle deformation upon substrate adhesion (Figure 2b). For CM particles this ratio was 0.73 ± 0.02 (standard error of the mean (s.e.m.), $N = 97$ particles), for VLDL the ratio was 0.95 ± 0.04 (s.e.m., $N = 56$), for LDL the ratio was 0.88 ± 0.05 (s.e.m., $N = 40$) and for HDL the ratio was 0.74 ± 0.04 (s.e.m., $N = 75$), indicating spreading upon substrate adhesion. Significant differences were identified between CM and VLDL, CM and LDL, HDL and VLDL and HDL and LDL (two-sided t-test, $p = 0.05$), showing that CM and HDL do deform more upon substrate adhesion compared to VLDL and LDL. Next the radius of the LPs before substrate adhesion, assuming surface area conservation, was determined. The determined radii confirm the expected size trend for the different LP classes: 65 ± 3 nm (s.e.m., $N = 97$ CM particles), 59 ± 3 nm (s.e.m., $N = 56$ VLDL particles), 43 ± 6 nm (s.e.m., $N = 40$ LDL particles) and 16 ± 1 nm (s.e.m., $N = 75$ HDL particles) for CM, VLDL, LDL and HDL, respectively (Figure 2c).

3.2 | Comparing the mechanical behavior of LPs and EVs

The mechanical properties of CM, VLDL, LDL and HDL were analyzed by nanoindentation experiments performed on individual particles. It was recently reported, that the mechanical response of EVs and liposomes during indentation is typically marked by an initial linear behavior followed by a subsequent flattening before pinching through the layers of membrane marked by two peaks before pushing on the substrate (Vorselen et al., 2017, 2018, 2018). In order to evaluate the effect of LPs in a sample that also

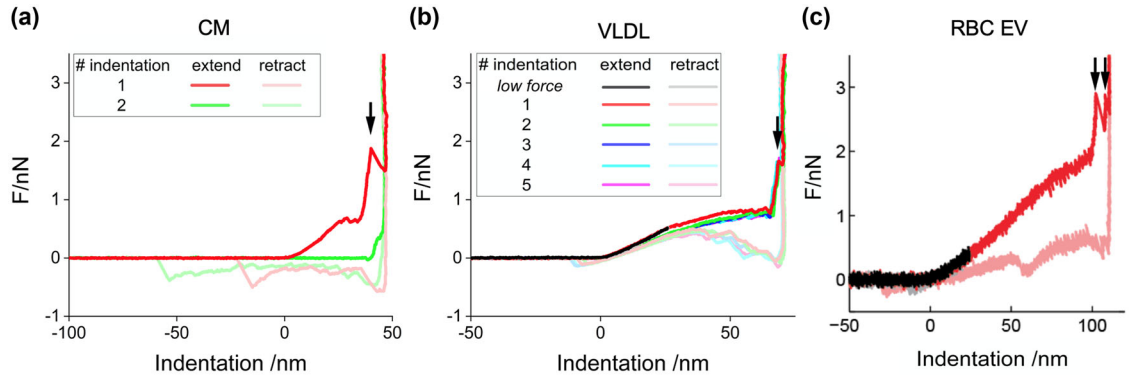

FIGURE 3 Typical force indentation curves (FDCs) on LPs and red blood cell (RBC) EVs. **(a)** Typical FDCs of multiple consecutive indentations on a chylomicron (CM) particle. **(b)** Typical FDCs of multiple consecutive indentations on a very-low density lipoprotein (VLDL) particle. **(c)** Two subsequent AFM FDCs on a RBC EV showing an initial linear elastic response (black and red curves) followed by a subtle flattening of the second FDC. Then an abrupt increase in stiffness occurs, followed by two break events (indicated by two black arrows), after which the glass surface (identified as a vertical line) is reached. The two break events correspond to the penetration of the lipid bilayers and the first one is typically larger than the second. Curves in a lighter color indicate the mechanical behavior during AFM tip retraction. The black extension and light grey retraction curve display a low force indentation curve demonstrating the reversible behavior of the RBC EV in the low force regime. Adapted from ref. (Vorselen et al., 2018) with permission from Nature Communications.

contains EVs, we applied the same Canham-Helfrich theory-based indentation model to the LPs. Figure 3 shows typical FDCs on CM and VLDL as well as a FDC recorded on a red blood cell EV. The features reported for EVs (linear increase in force, subsequent flattening and penetration of layer) can also be observed for LPs. Throughout the experiments we found LPs with only one penetration event occurring close to the substrate, instead of two for EVs (black arrows in Figure 3). To examine whether the number of penetration/break events close to the substrate could be used to differentiate between LPs and EVs, we analyzed the number of penetration events occurring up to 10 nm from the substrate and the break size of the LPs (Supplementary Figure 2). The majority of LPs showed 1 or 2 break events, evenly distributed for CM and HDL (Supplementary Figure 2a). In contrast, more VLDL exhibited 2 break events than 1, while LDL showed the opposite trend and additionally exhibited a considerable amount with 3 break events (Supplementary Figure 2a). Determining the break sizes of the LPs we found a wide distribution (Supplementary Figure 2b).

3.3 | Most CM collapse after first indentation

CM particles typically already collapsed after the initial low force (~0.4 nN) indentation, as revealed by the height extracted from the second FDC and confirmed by imaging after indentation. Therefore, we adjusted the experimental procedure for CM and indented these LPs directly with a maximum force to capture the particle's whole response. Typical AFM images of CM and the other LPs before and after indentation are shown in Supplementary Figure 3. Previous indentation studies on liposomes and natural vesicles reported reversibility, with either no detectable change in geometry of the vesicles (Calò et al., 2014; Li et al., 2011), or a recovery of ~60 % in the case of red blood cell EVs (Vorselen et al., 2018). The higher tendency of rupture events for CM during the experiments was compared to the behavior of the other classes of LPs. Typically, VLDL, LDL and HDL do not break after a low force indentation, but they can break after high force indentation. To study this systematically we determined after how many consecutive indentations the first decrease in height occurred. Figure 4 shows the results obtained for all four classes of LPs. About 96 % of CM indented showed a clear height change after the first indentation, while at the other extreme ~50 % of the VLDL showed reversible behavior even after 5 indentations.

3.4 | CM and VLDL are softer than LDL

Next, we characterized the LPs mechanically. Vorselen et al. (Vorselen et al., 2017) developed a model based on Canham-Helfrich theory demonstrating that the mechanical properties of adherent fluid vesicles are governed by membrane bending and internal osmotic pressure. With this model the bending modulus can be estimated using the vesicle stiffness, radius and tether force. In order to evaluate possible effects of LPs in EV samples the same model was applied to the LP classes investigated in this study. The height of the particles was both determined from the AFM image as from the FDC, revealing comparable results (Supplementary Figure 4).

To ensure indentation on the particle's center, only particles with height from FDC ≥ height from AFM image were included. LP stiffness was determined by fitting the initial linear response for indentations from 0.02 R_c up to 0.1 R_c. The stiffness of the

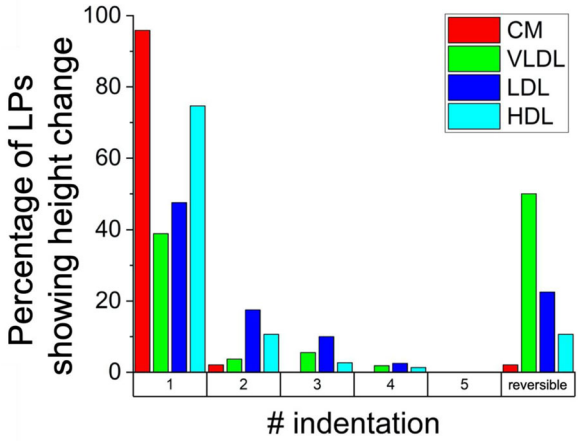

FIGURE 4 Multiple indentations analyzed for height change. Lipoproteins (LPs) were indented 5 times each. x-axis displays the indentation number after which the first height change appeared. Category 'reversible' represents particles that did not exhibit a height change in the 5 FDCs recorded. Chylomicrons (CM): $N = 97$; very-low density lipoproteins (VLDL): $N = 56$; low-density lipoproteins (LDL): $N = 40$; high-density lipoproteins (HDL): $N = 75$

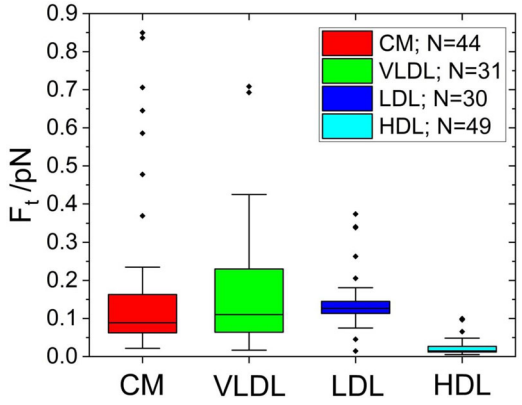

FIGURE 5 Tether forces F_t of the different lipoprotein (LP) classes. Boxplots are shown in which the line within the box indicates median, box limits indicate upper and lower quartiles and whiskers indicate 1.5× interquartile range. Average tether force for chylomicrons (CM) was $F_t = 179 \pm 33$ pN (s.e.m., $N = 44$), very-low density lipoprotein (VLDL) particles show a mean tether force $F_t = 177 \pm 31$ pN (s.e.m., $N = 31$), low-density lipoprotein (LDL) particles show an average tether force $F_t = 149 \pm 15$ pN (s.e.m., $N = 30$), and high-density lipoprotein (HDL) particles show significantly lower tether forces ($F_t = 24 \pm 3$ pN, s.e.m., $N = 49$), respectively. The tether forces of 2 CM, 20 VLDL and 4 LDL could not be measured as their tether lengths exceeded the recorded length of force indentation curves (FDCs).

different LP samples did not show any significant difference (Supplementary Figure 5), revealing that stiffness cannot be used as a parameter to distinguish between the particles. More importantly, stiffness is an extrinsic property that also depends on the particle size and pressurization and does not necessarily reflect intrinsic differences between the different LP types. In contrast, bending modulus is an intrinsic property of the membrane (Vorselen et al., 2017).

To evaluate the tether formation and forces, the retrace of indentation curves was analyzed. A tether was detected in the retrace in ~47 % of FDCs of CM, ~82 % of FDCs of VLDL and ~75 % of FDCs of LDL, respectively (Table 1). In ~65 % of FDCs recorded on HDLs a tether was observed, however, due to the small particle size, the tethers were relatively short. The average tether forces F_t of the different LP classes are shown in Figure 5. Multiple CM, VLDL and LDL formed tethers longer than the recorded FDC in which cases no tether force could be determined. Using the information on F_t, R_c and k we applied the model introduced by Vorselen et al. (Vorselen et al., 2017, 2020) to determine the bending modulus of CM, VLDL and LDL. Due to the small size and deformability of HDL particles, and hence the difficulty to distinguish deformed particles from collapsed particles, we could not determine the bending modulus for HDL. The bending modulus of CM is $5 \pm 1\ k_BT$ (s.e.m., $N = 44$). The bending modulus of VLDL is $5 \pm 2\ k_BT$ (s.e.m., $N = 31$), and the bending modulus of LDL is $10 \pm 2\ k_BT$ (s.e.m., $N = 30$). This reveals that the bending modulus of LDL is double the value of the bending moduli of VLDL and CM particles. Hence, LDL have a significantly more rigid lipid shell than VLDL and CM.

TABLE 1 Overview of results obtained in this study. The numbers of particles analyzed are indicated. Displayed are values obtained for the deformation upon substrate adhesion defined by H/R_c, calculated radii on solution R_0, percentages for LPs showing height changes after the first high force indentation and reversibility, stiffness k, tether forces F_t, probabilities of tether formation and bending moduli of lipoprotein particles. The probability of tether formation is quantified by the number of particles showing a tether in the retract curve of analyzed indentation cycle divided by the total number of particles fulfilling the analysis criteria (see also Ref. Vorselen et al., 2020). Bending moduli were determined using atomic force microscopy (AFM) nanoindentation approach.

	CM	VLDL	LDL	HDL
Deformation upon substrate adhesion H/R_c (mean ± s.e.m.)[1]	0.73 ± 0.02 ($N = 97$)	0.95 ± 0.04 ($N = 56$)	0.88 ± 0.05 ($N = 40$)	0.74 ± 0.04 ($N = 75$)
Radius before substrate adhesion R_0 (mean ± s.e.m.)	65 ± 3 nm ($N = 97$)	59 ± 3 nm ($N = 56$)	43 ± 6 nm ($N = 40$)	16 ± 1 nm ($N = 75$)
LPs showing height change after first high force indentation	96 %	39 %	48 %	75 %
Reversibility	2 %	50 %	23 %	11 %
Stiffness k (mean ± s.e.m.)	0.017 ± 0.001 N/m ($N = 97$)	0.019 ± 0.002 N/m ($N = 56$)	0.016 ± 0.001 N/m ($N = 40$)	0.014 ± 0.001 N/m ($N = 71$)
Probability of tether formation	48 %	82 %	48 %	75 %
Tether force F_t (mean ± s.e.m.)	179 ± 33 pN ($N = 44$)	177 ± 31 pN ($N = 31$)	149 ± 15 pN ($N = 30$)	24 ± 3 pN ($N = 49$)
Bending modulus	5 ± 1 k_BT ($N = 44$)	5 ± 2 k_BT ($N = 31$)	10 ± 2 k_BT ($N = 30$)	not analyzed due to minute size of HDL

[1]CM: Chylomicrons; VLDL: very-low density lipoproteins; LDL: low-density lipoproteins, s.e.m.: standard error of the mean.

4 | DISCUSSION

This study provides an in-depth examination of the mechanical properties of LPs. The results obtained are summarized in Table 1. By means of AFM imaging, we extracted the size of LPs in solution confirming expected size trends. Literature values on LP sizes as obtained by ion mobility analysis, a more indirect method to determine the size of LPs, reported smaller sizes for the LPs than in our AFM analysis (Caulfield et al., 2008). In contrast, nuclear magnetic resonance analysis (NMR) yielded similar sizes for CM and VLDL as our AFM analysis, while the radii obtained for LDL and HDL were larger than the values reported here (Jeyarajah et al., 2006).

We have shown that the mechanical behavior of LPs exhibits qualitative similarities to that of EVs measured previously (Figure 3). A quantitative analysis reveals additional similarities: EVs typically show two penetration events at the end of the FDCs, while LPs typically show one or two events. Although the number of penetrations cannot be used to unambiguously distinguish all LPs from EVs, a partial distinction can be made and thereby it can be identified whether there are LPs in a sample of EVs. Next to the number of penetrations, also the break size was analysed. While the break size of liposomes could be clearly used to identify their degree of lamellarity (Vorselen et al., 2018), we did not find such unambiguous behavior for LPs. To use this information for differentiation between LPs and EVs further studies are needed, extending the current knowledge from liposomes to EVs. Furthermore, CM collapse after the first indentation irrespective of the applied force, while EVs typically do not show this behavior. Due to the minute size of the adhered HDL (~13 nm), their bending modulus could not be determined, as the particles had likely collapsed during adhesion to the substrate. Previous studies of AFM measurements on HDL and LDL reported small recorded height of less than 10 nm (Gan et al., 2015, Wang et al., 2020). This indicates that the particles probably collapsed on the surface in those studies. The observation that HDL likely collapses on the surface fits with our data. In contrast, the LDL particles did not collapse in our experiments. This is probably due to differences in surface treatment and imaging parameters between these studies.

Looking at the probability of tether formation, the values of the LPs are in the range of reported probabilities of EVs (Vorselen et al., 2018). Also, the bending moduli of CM, VLDL and LDL (~5-10 k_BT) are in the range of EVs as determined by AFM nanoindentation (~6-15 k_BT) (Sorkin et al., 2018; Vorselen et al., 2018). Different approaches investigating the mechanics of membranes, e.g. RBC membrane using flicker spectroscopy (~15 k_BT), micropipette aspiration and tether pulling experiments (~40 k_BT) and optical tweezers assisted measurements of membrane fluctuations (~60 k_BT) typically showed higher values than for LPs (Betz et al., 2009; Brochard & Lennon, 1975; Butler et al., 2008; Duwe et al., 1990; Evans, 1983; Park et al., 2010).

Comparing the LP samples, we find that CM and VLDL show a bending modulus about 50 % lower than LDL (10 ± 2 k_BT). This could be related to differences in lipid and/or (apolipo)protein composition (Figure 1), fitting with the suggestion that the physical properties, apolipoprotein distribution and functioning, e.g. plasma membrane protein activity, are governed by the lipids in the surface monolayer of lipoproteins (Massey & Pownall, 1998). In particular, cholesterol and cholesteryl esters in

lipoprotein particles may affect the physicochemical properties. The relative cholesterol content of the LDL fraction (~50 %) is much higher than in VLDL and CM. In contrast, the difference in cholesterol content of CM (~3 % cholesterol) and VLDL (~20 % cholesterol) does not lead to a difference in bending modulus. Phosphatidylcholine (PC) is the main lipid present in the monolayer of plasma LPs with differentiation among different LP classes (Massey & Pownall, 1998), for example, LDL were shown to contain more saturated PC, sphingomyelin, and unesterified cholesterol than HDL leading to different molecular packing in the LP's surfaces (Ibdah et al., 1989). Knowing that the properties of the lipid acyl chains (e.g. degree of (un)saturation, length) affect the mechanical properties of membranes (lipid bilayer), i.e. the bending modulus directly depends on membrane thickness (Vanni et al., 2019; Zimmerberg & Kozlov, 2006), it could be a possible explanation of the differences in bending moduli observed for LPs (lipid monolayer) in this study. In line with decreasing (protein + free cholesterol)/phospholipid ratio in the LPs the surface fluidity increased from HDL to LDL and VLDL (Massey & Pownall, 1998). As membrane fluidity is known to affect the mechanical behavior of EVs (Vorselen et al., 2017), the differences observed in LPs could have an impact on the bending modulus as well. However, as previously reported (Vorselen et al., 2018), (apolipo)proteins themselves can have significant influence on the stiffness of EVs and LPs. The different content of apolipoproteins in CM/VLDL and LDL could therefore also affect the stiffness of the particles and consequently their bending modulus.

Previous studies on native and oxidized LDL reported smaller particles and a reduced Young's modulus under acidic conditions compared to neutral environment (Wang et al., 2020, 2021). The oxidized form of LDL (oxLDL) is a known risk factor in atherosclerosis. At pH 7.4 oxLDL were reported to be smaller, softer (Young's modulus) and to have higher adhesive forces than native LDL explaining enhanced infiltration, enhanced adhesion and accumulation of oxLDL on the endothelium/extracellular matrix observed in atherosclerosis (Wang et al., 2020).

Considering all information obtained to evaluate whether an EV sample is contaminated with LPs we found that the mechanical characterization can contribute to distinguish between LPs and EVs. The size and deformability of HDL led to an exclusion parameter of this particle class when measuring EVs. CM showed an almost 100 % probability of rupturing after the first, low force indentation, which is not common for EVs (Vorselen et al., 2018). As such the presence or absence of height change/collapse after a low force indentation represents a clear distinction between CM and EVs. In addition, VLDL were softer than LDL and most measured EVs, while LDL showed a number of similarities with EVs, for example size and bending modulus, but also some differences. A partial, but not complete, differentiation between VLDL/LDL and EVs could be made by analyzing the penetration events. For a complete distinction between these particles in a sample mixed of EVs and LDL, further characterization is needed. Enciso-Martinez et al. (Enciso-Martinez et al., 2020) investigated the same CM and VLDL samples studied here and demonstrated the identification of LPs in a mixed sample using a non-destructive label-free Rayleigh-Raman method. A similar approach might be possible for identifying LDL.

To conclude, we have shown new results on the structural and material properties of LPs using an innovative AFM nanoindentation approach, previously applied to EVs. We found that the mechanical characteristics of CM and VLDL are significantly different from LDL. The increased bending modulus of LDL fits with the cholesterol content of this particle class (Evans & Needham, 1987; Evans & Rawicz, 1990; Rawicz et al., 2000), while our results on CM and VLDL suggest an additional influence of apolipoprotein content to the rigidity of LPs. Furthermore, our approach allows to reveal whether there is LP contamination in EV samples, which is particularly useful when evaluating (new) procedures to isolate EVs from plasma. Hereby our data yields new information on the mechanical information of nano-sized LPs and their differences/similarities with EVs. This information helps to understand uptake processes and is potentially useful in designing/optimizing drug delivery approaches. Furthermore, the applied method can be more broadly used, for example to study LPs in dyslipidemia and diabetes.

AUTHOR CONTRIBUTIONS

Wouter H. Roos: Conceptualization; Funding acquisition; Methodology; Resources; Supervision; Validation; Writing – original draft; Writing – review & editing. Melissa C. Piontek: Conceptualization; Data curation; Formal analysis; Investigation; Methodology; Validation; Visualization; Writing - original draft; Writing - review & editing.

ACKNOWLEDGEMENTS

The authors would like to thank Leon Terstappen and Agustin Enciso-Martinez for the kind gift of lipoprotein samples. We also thank Edwin van der Pol for critical feedback on the manuscript. We thank Sourav Maity and Sajitha Sasidharan for support and discussion. W.H.R. acknowledges support via a NWO Vidi grant and the STW Cancer-ID program (project 14192).

CONFLICT OF INTEREST

The authors report no conflict of interest.

DATA AVAILABILITY STATEMENT

The data supporting the findings of this study are available from the corresponding authors on request.

ORCID

Melissa C. Piontek https://orcid.org/0000-0003-3304-8919

REFERENCES

Betz, T., Lenz, M., Joanny, J. - F., & Sykes, C. (2009). ATP-dependent mechanics of red blood cells. *Proceedings of the National Academy of Sciences*, *106*, 15320–15325. https://doi.org/10.1073/pnas.0904614106

Brochard, F., & Lennon, J. F. (1975). Frequency spectrum of the flicker phenomenon in erythrocytes. *Journal De Physique*, *36*, 1035–1047. https://doi.org/10.1051/jphys:0197500360110103500

Busatto, S., Yang, Y., Iannotta, D., Davidovich, I., Talmon, Y., & Wolfram, J. (2022). Considerations for extracellular vesicle and lipoprotein interactions in cell culture assays. *Journal of Extracellular Vesicles*, 11. https://doi.org/10.1002/jev2.12202

Butler, J., Mohandas, N., & Waugh, R. E. (2008). Integral protein linkage and the bilayer-skeletal separation energy in red blood cells. *Biophysical Journal*, *95*, 1826–1836. https://doi.org/10.1529/biophysj.108.129163

Calò, A., Reguera, D., Oncins, G., Persuy, M. - A., Sanz, G., Lobasso, S., Corcelli, A., Pajot-Augy, E., & Gomila, G. (2014). Force measurements on natural membrane nanovesicles reveal a composition-independent, high Young's modulus. *Nanoscale*, *6*, 2275. https://doi.org/10.1039/c3nr05107b

Caulfield, M. P., Li, S., Lee, G., Blanche, P. J., Salameh, W. A., Benner, W. H., Reitz, R. E., & Krauss, R. M. (2008). Direct determination of lipoprotein particle sizes and concentrations by ion mobility analysis. *Clinical Chemistry*, *54*, 1307–1316. https://doi.org/10.1373/clinchem.2007.100586

Chaudhary, J., Bower, J., & Corbin, I. R. (2019). Lipoprotein drug delivery vehicles for cancer: Rationale and reason. *International Journal of Molecular Sciences*, 20. https://doi.org/10.3390/ijms20246327

Chiva-Blanch, G., & Badimon, L. (2019). Cross-talk between lipoproteins and inflammation: The role of microvesicles. *Journal of Clinical Medicine*, *8*. https://doi.org/10.3390/jcm8122059

Coumans, F. A. W., Brisson, A. R., Buzas, E. I., Dignat-George, F., Drees, E. E. E., El-Andaloussi, S., Emanueli, C., Gasecka, A., Hendrix, A., Hill, A. F., Lacroix, R., Lee, Y., Van Leeuwen, T. G., Mackman, N., Mäger, I., Nolan, J. P., Van Der Pol, E., Pegtel, D. M., Sahoo, S., … Nieuwland, R. (2017). Methodological guidelines to study extracellular vesicles. *Circulation Research*, *120*, 1632–1648. https://doi.org/10.1161/CIRCRESAHA.117.309417

Duwe, H. P., Kaes, J., & Sackmann, E. (1990). Bending elastic moduli of lipid bilayers: Modulation by solutes. *Journal De Physique*, *51*, 945–961. https://doi.org/10.1051/jphys:019900051010094500

Enciso-Martinez, A., Van Der Pol, E., Hau, C. M., Nieuwland, R., Van Leeuwen, T. G., Terstappen, L. W. M. M., & Otto, C. (2020). Label-free identification and chemical characterisation of single extracellular vesicles and lipoproteins by synchronous Rayleigh and Raman scattering. *Journal of Extracellular Vesicles*, *9*. https://doi.org/10.1080/20013078.2020.1730134

Evans, E., & Needham, D. (1987). Physical properties of surfactant bilayer membranes: Thermal transitions, elasticity, rigidity, cohesion, and colloidal interactions. *Journal of Physical Chemistry*, *91*, 4219–4228. https://doi.org/10.1021/j100300a003

Evans, E., & Rawicz, W. (1990). Entropy-driven tension and bending elasticity in condensed-fluid membranes. *Physical Review Letter*, *64*, 2094–2099. https://doi.org/10.1103/PhysRevLett.64.2094

Evans, E. A. (1983). Bending elastic modulus of red blood cell membrane derived from buckling instability in micropipet aspiration tests. *Biophysical Journal*, *43*, 27–30. https://doi.org/10.1016/S0006-3495(83)84319-7

Gan, C., Ao, M., Liu, Z., & Chen, Y. (2015). Imaging and force measurement of LDL and HDL by AFM in air and liquid. *FEBS Open Bio*, *5*, 276–282. https://doi.org/10.1016/j.fob.2015.03.014

Ibdah, J. A., Lund-Katz, S., & Phillips, M. C. (1989). Molecular packing of high-density and low-density lipoprotein surface lipids and apolipoprotein A-I binding. *Biochemistry*, *28*, 1126–1133. https://doi.org/10.1021/bi00429a029

Jeyarajah, E. J., Cromwell, W. C., & Otvos, J. D. (2006). Lipoprotein particle analysis by nuclear magnetic resonance spectroscopy. *Clinics in Laboratory Medicine*, *26*, 847–870. https://doi.org/10.1016/j.cll.2006.07.006

Kocar, E., Rezen, T., & Rozman, D. (2021). Cholesterol, lipoproteins, and COVID-19: Basic concepts and clinical applications. *BBA Molecular and Cell Biology of Lipids*, *1866*, 158849.

Kostner, G. M., & Laggner, P. 2019. Chapter 2. Chemical and Physical Properties of Lipoproteins, In J.C. Fruchart, J. Shepherd (Eds.), *Hum. Plasma Lipoproteins*, De Gruyter, Berlin, pp. 23–54. https://doi.org/10.1515/9783110873665-005

Li, S., Eghiaian, F., Sieben, C., Herrmann, A., & Schaap, I. A. T. (2011). Bending and puncturing the influenza lipid envelope. *Biophysical Journal*, *100*, 637–645. https://doi.org/10.1016/j.bpj.2010.12.3701

Massey, J. B., & Pownall, H. J. (1998). Surface properties of native human plasma lipoproteins and lipoprotein models. *Biophysical Journal*, *74*, 869–878. https://doi.org/10.1016/S0006-3495(98)74010-X

Park, Y., Best, C. A., Badizadegan, K., Dasari, R. R., Feld, M. S., Kuriabova, T., Henle, M. L., Levine, A. J., & Popescu, G. (2010). Measurement of red blood cell mechanics during morphological changes. *Proceedings of the National Academy of Sciences*, *107*, 6731–6736. https://doi.org/10.1073/pnas.0909533107

Pownall, H. J., Rosales, C., Gillard, B. K., & Gotto, A. M. (2021). High-density lipoproteins, reverse cholesterol transport and atherogenesis. *Nature Reviews Cardiology*, *18*, 712–723. https://doi.org/10.1038/s41569-021-00538-z

Ramirez, M. I., Amorim, M. G., Gadelha, C., Milic, I., Welsh, J. A., Freitas, V. M., Nawaz, M., Akbar, N., Couch, Y., Makin, L., Cooke, F., Vettore, A. L., Batista, P. X., Freezor, R., Pezuk, J. A., Rosa-Fernandes, L., Carreira, A. C. O., Devitt, A., Jacobs, L., … Dias-Neto, E. (2018). Technical challenges of working with extracellular vesicles. *Nanoscale*, *10*, 881–906. https://doi.org/10.1039/c7nr08360b

Rawicz, W., Olbrich, K. C., McIntosh, T., Needham, D., & Evans, E. A. (2000). Effect of chain length and unsaturation on elasticity of lipid bilayers. *Biophysical Journal*, *79*, 328–339. https://doi.org/10.1016/S0006-3495(00)76295-3

Roos, W. H., Bruinsma, R., & Wuite, G. J. L. (2010). Physical virology. *Nature Physics*, *6*, 733–743. https://doi.org/10.1038/nphys1797

Simonsen, J. B. (2017). What are we looking at? Extracellular vesicles, lipoproteins, or both? *Circulation Research*, *121*, 920–922. https://doi.org/10.1161/CIRCRESAHA.117.311767

Sódar, B. W., Kittel, Á., Pálóczi, K., Vukman, K. V., Osteikoetxea, X., Szabó-Taylor, K., Németh, A., Sperlágh, B., Baranyai, T., Giricz, Z., Wiener, Z., Turiák, L., Drahos, L., Pállinger, É., Vékey, K., Ferdinandy, P., Falus, A., & Buzás, E. I. (2016). Low-density lipoprotein mimics blood plasma-derived exosomes and microvesicles during isolation and detection. *Scientific Reports*, *6*, 1–12. https://doi.org/10.1038/srep24316

Sorkin, R., Huisjes, R., Boškovic, F., Vorselen, D., Pignatelli, S., Ofir-Birin, Y., Leal, J. K. F., Schiller, J., Mullick, D., Roos, W. H., Bosman, G., Regev-Rudzki, N., Schiffelers, R. M., & Wuite, G. J. L. (2018). Nanomechanics of extracellular vesicles reveals vesiculation pathways. *Small*, *1801650*, 1–8. https://doi.org/10.1002/smll.201801650

Sorkin, R., Marchetti, M., Logtenberg, E., Piontek, M. C., Kerklingh, E., Brand, G., Voleti, R., Rizo, J., Roos, W. H., Groffen, A. J., & Wuite, G. J. L. (2020). Synaptotagmin-1 and Doc2b exhibit distinct membrane-remodeling mechanisms. *Biophysical Journal*, *118*, 1–14. https://doi.org/10.1016/j.bpj.2019.12.021

Sun, Y., Saito, K., & Saito, Y. (2019). Lipid profile characterization and lipoprotein comparison of extracellular vesicles from human plasma and serum. *Metabolites*, *9*, 10–14. https://doi.org/10.3390/metabo9110259

Théry, C., Witwer, K. W., Aikawa, E., Alcaraz, M. J., Anderson, J. D., Andriantsitohaina, R., Antoniou, A., Arab, T., Archer, F., Atkin-Smith, G. K., Ayre, D. C., Bach, J. - M., Bachurski, D., Baharvand, H., Balaj, L., Baldacchino, S., Bauer, N. N., Baxter, A. A., Bebawy, M., … Zuba-Surma, E. K. (2018). Minimal information for studies of extracellular vesicles 2018 (MISEV2018): A position statement of the International Society for Extracellular Vesicles and update of the MISEV2014 guidelines. *Journal of Extracellular Vesicles*, *7*. https://doi.org/10.1080/20013078.2018.1535750

van der Pol, E., Coumans, F. A. W., Grootemaat, A. E., Gardiner, C., Sargent, I. L., Harrison, P., Sturk, A., & van Leeuwen, T. G., Nieuwland, R. (2014). Particle size distribution of exosomes and microvesicles determined by transmission electron microscopy, flow cytometry, nanoparticle tracking analysis, and resistive pulse sensing. *Journal of Thrombosis and Haemostasis*, *12*, 1182–1192. https://doi.org/10.1111/jth.12602

Vanni, S., Riccardi, L., Palermo, G., & De Vivo, M. (2019). Structure and dynamics of the acyl chains in the membrane trafficking and enzymatic processing of lipids. *Accounts of Chemical Research*, *52*, 3087–3096. https://doi.org/10.1021/acs.accounts.9b00134

Vorselen, D., MacKintosh, F. C., Roos, W. H., & Wuite, G. J. L. (2017). Competition between bending and internal pressure governs the mechanics of fluid nanovesicles. *ACS Nano*, *11*, 2628–2636. https://doi.org/10.1021/acsnano.6b07302

Vorselen, D., Marchetti, M., López-iglesias, C., Peters, P. J., Roos, W. H., & Wuite, G. J. L. (2018). Multilamellar nanovesicles show distinct mechanical properties depending on their degree of lamellarity. *Nanoscale*, *10*, 5318–5324. https://doi.org/10.1039/c7nr09224e

Vorselen, D., Piontek, M. C., Roos, W. H., & Wuite, G. J. L. (2020). Mechanical characterization of liposomes and extracellular vesicles, a protocol, front. *Molecular Biosciences*, *7*, 1–14. https://doi.org/10.3389/fmolb.2020.00139

Vorselen, D., van Dommelen, S. M., Sorkin, R., Piontek, M. C., Schiller, J., Döpp, S. T., Kooijmans, S. A. A., van Oirschot, B. A., Versluijs, B. A., Bierings, M. B., van Wijk, R., Schiffelers, R. M., Wuite, G. J. L., & Roos, W. H. (2018). The fluid membrane determines mechanics of erythrocyte extracellular vesicles and is softened in hereditary spherocytosis. *Nature Communications*, *9*. https://doi.org/10.1038/s41467-018-07445-x

Wang, K., Gan, C., Wang, H., Ao, M., Fan, Y., & Chen, Y. (2021). AFM detects the effects of acidic condition on the size and biomechanical properties of native/oxidized low-density lipoprotein. *Colloids Surfaces B Biointerfaces*, *208*, 112053. https://doi.org/10.1016/j.colsurfb.2021.112053

Wang, K., Li, Y., Luo, C., & Chen, Y. (2020). Dynamic AFM detection of the oxidation-induced changes in size, stiffness, and stickiness of low-density lipoprotein. *Journal of Nanobiotechnology*, *18*, 1–10. https://doi.org/10.1186/s12951-020-00727-x

Zimmerberg, J., & Kozlov, M. M. (2006). How proteins produce cellular membrane curvature. *Nature Reviews Molecular Cell Biology*, *7*, 9–19. https://doi.org/10.1038/nrm1784

SUPPORTING INFORMATION

Additional supporting information can be found online in the Supporting Information section at the end of this article.

How to cite this article: Piontek, M. C., & Roos, W. H. (2022). Lipoprotein particles exhibit distinct mechanical properties. *Journal of Extracellular Biology*, *1,* e68. https://doi.org/10.1002/jex2.68